MAX-PLANCK-INSTITUT FÜR PHYSIK

WERNER-HEISENBERG-INSTITUT

MPI-PhE/94-34
PITHA 94-51 RWTH Aachen
HD-IHEP 94-07

November 1994

Study of a Novel Electromagnetic Liquid Argon Calorimeter

- The TGT -

RD33 Collaboration

RWTH Aachen, *CERN*, *JINR* Dubna, Universität Heidelberg, *IEP* Košice,
MPI München, *IHEP* Protvino

80805 München · Föhringer Ring 6

Study of a Novel Electromagnetic Liquid Argon Calorimeter

– The TGT –

C. Berger, W. Braunschweig, E. Geulig, M. Schöntag, R. Siedling, M. Wlochal
I. Physikalisches Institut der RWTH Aachen, Germany

A. Putzer[1], J. Wotschack
CERN, Geneva, Switzerland

A. Cheplakov, A. Feshchenko, M. Kazarinov, V. Kukhtin, E. Ladygin, V. Obudovskij
Joint Institute for Nuclear Research, Dubna, Russia

C. Geweniger, P. Hanke, E.-E. Kluge, J. Krause, M. Schmidt, H. Stenzel, K. Tittel, M. Wunsch, D. Zerwas
Institut für Hochenergiephysik der Universität Heidelberg, Germany

D. Bruncko, A. Jusko, B. Kocper, M. Lupták
Institute of Experimental Physics, Slovak Academy of Sciences, Košice, Slovak Republic

M. Aderholz, J. Bán[2], H. Brettel, F. Dydak[3], J. Fent, H. Frey, J. Huber, K. Jakobs, C. Kiesling, A.E. Kiryunin[4], H. Oberlack, P. Ribarics, P. Schacht, U. Stiegler[5]
Max-Planck-Institut für Physik, München, Germany

M.Y. Bogolyubsky, O.V. Buyanov, S.V. Chekulaev, L.L. Kurchaninov, M.S. Levitsky, V.V. Maximov, A.A. Minaenko, A.M. Moiseev, P.A. Semenov, V.V. Tikhonov
Institute for High Energy Physics, Protvino, Russia

U. Straumann
Physikalisches Institut der Universität Zürich, Switzerland

(Submitted to *Nuclear Instruments & Methods* **A**)

[1] On leave of absence from Universität Heidelberg.
[2] Permanent address: IEP Košice, Slovak Republic.
[3] Also at CERN.
[4] Permanent address: IHEP Protvino, Russia.
[5] Now at CERN.

Abstract

The concept and the basic design of a fast, highly granular and compact electromagnetic liquid argon calorimeter are described. This novel calorimeter offers uniform energy response and constant energy resolution independent of the production angle of an impinging particle and of its impact position at the calorimeter. An example of a calorimeter with full rapidity coverage in an application in a collider detector is given. An important aspect of the concept is the electronics for fast signal processing matched to the short charge collection time. We report on the experience with the realization of a prototype calorimeter module and on its performance in a testbeam exposure.

1 Introduction

During the last decade, the liquid argon (LAr) technique for calorimetry has become a mature technology. It is a good candidate for both the electromagnetic and the hadronic calorimetry of future collider detectors, especially since its active medium is radiation hard [1]. It offers good reproducibility of charge collection, accurate and time stable energy calibration, linearity of the signal response, and easy adaptation of fine granularity to the requirements of the experiment. It has been demonstrated that large LAr systems can be realized [2], [3]. LAr calorimeters can be operated in magnetic fields and allow easy and reliable handling during the experiment. Recently it has been demonstrated that the LAr calorimetry can yield fast signals [4].

However, most existing LAr calorimeters have severe drawbacks: They are constructed in a monolithic manner, making a test complicated prior to the final assembly of the complete structure. In a collider experiment, it is difficult to realize a pointing geometry in all three dimensions; therefore the sampling changes as function of impact position and direction. Relatively large LAr gaps imply operation at high voltages, large dimensions and a large effective radiation length.

In the present article a novel concept of a LAr calorimeter is presented, the thin gap turbine (TGT) calorimeter. It tries to overcome the shortcomings described above. It provides a compact and mechanically simple structure of a calorimeter stack of parallel plates with a high degree of modularity of individual absorber cells, a high degree of flexibility for the segmentation of the readout towers, and the means to deal with the fast signal processing of a large number of readout channels. The electronics is placed close to the pads in the liquid to keep the signal leads between the readout pad and the amplifier short in order to get the signals out quickly. For many applications, this implies to employ specially designed, radiation hard electronics.

In order to investigate the feasibility of the TGT concept and to develop the techniques for both the calorimeter structure and for the electronic signal processing, an R&D project [5] was launched as part of the overall R&D programme at CERN. It is carried out in two steps. In the first step the mechanical and electrical aspects of module construction are the primary goal: A test module is constructed; it is exposed to a testbeam using relatively slow electronics located in the cold argon gas. In the second phase this test module is equipped with TGT specific electronics using VLSI chips and current-sensitive amplifiers.

In this paper, the concept and the salient features of the TGT calorimeter and its electronics are discussed. We report on the first phase of the R&D project, in particular on the experience in constructing such a calorimeter, on the results obtained when summing several amplifiers into one readout channel and when calibrating it. Finally, first results from the analysis of data obtained from exposures to a testbeam are presented.

2 The TGT Calorimeter

2.1 The Concept

In collider experiments the calorimeter has to cover almost the full solid angle. Within its acceptance the response and the resolution should be as uniform as possible. In Fig. 1 the TGT concept and in Fig. 2 a possible implementation in a collider set-up are schematically shown. The geometrical set-up is such that any particle produced at the interaction point crosses individual absorber elements of flat plates with pad readout under a fixed angle (typically 45°). This guarantees constant thickness of both the absorber and the active gap within the entire calorimeter, thus optimizing the homogeneity of the response and minimizing any variation of the energy resolution within the full solid angle. In particular, transition zones are avoided where orientation or thickness of the absorber plates might otherwise have to change.

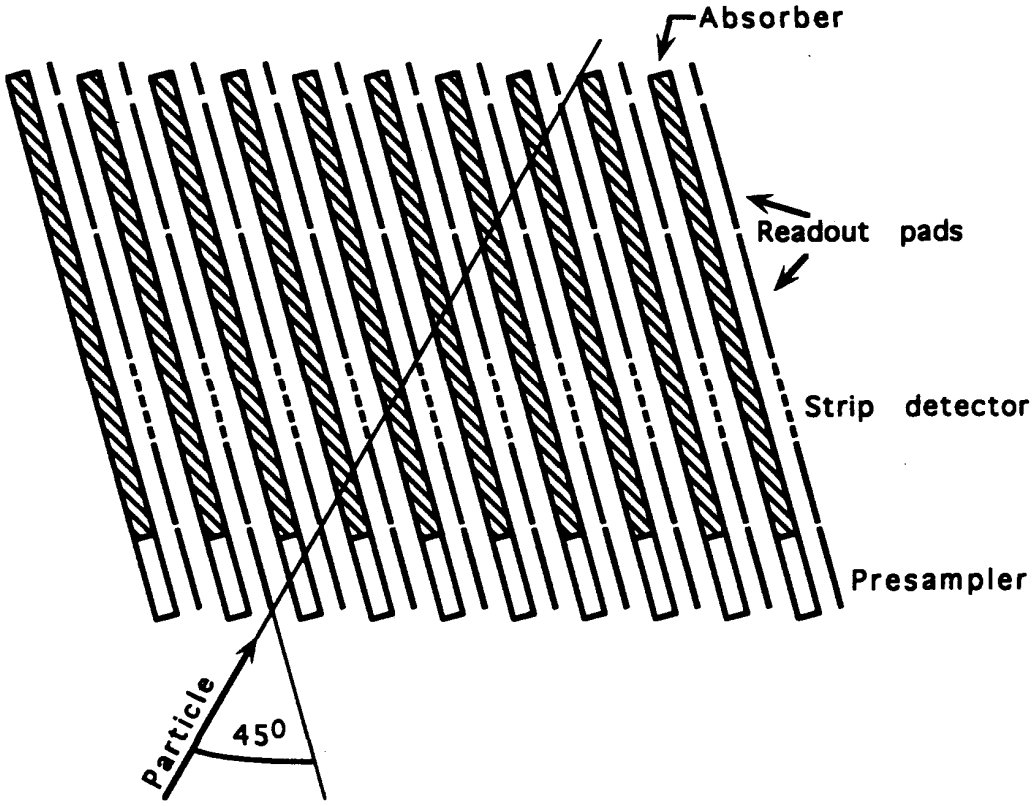

Figure 1: Schematic representation of the TGT concept.

The high energy of secondary particles produced in experiments at high center of mass energies asks for a dense and compact calorimeter to limit the size - and thus the cost - and/or the amount of energy leaking. In the TGT concept, the LAr gap is chosen to be rather small (e.g. 0.8 mm), yielding a high degree of compactness. In LAr calorimeters which are exposed to extremely high energy densities, space charge effects due to the low mobility of positive ions could deteriorate the signal. The small gap size minimizes this effect. In addition, a smaller LAr gap allows for a reduced high voltage and for small electrical guard zones around mechanical structures. This improves the homogeneity of the response and reduces the constant term in the energy resolution.

A further important TGT feature is its high degree of modularity: Individual modules ("absorber

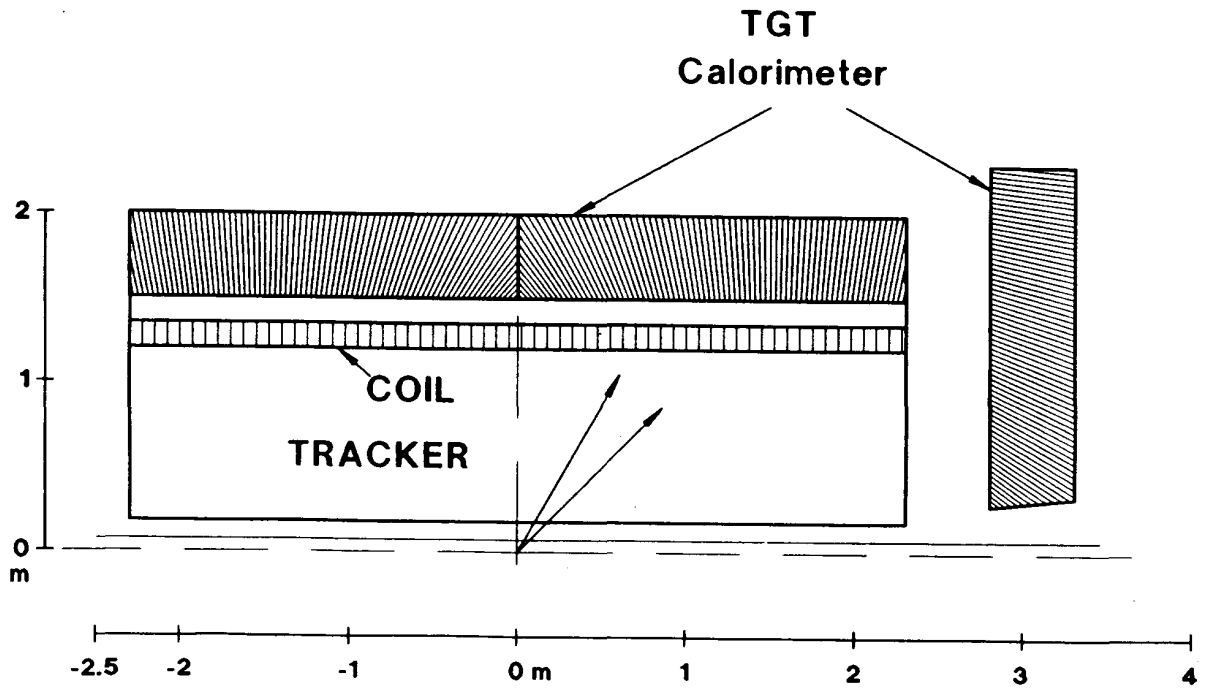

Figure 2: Schematic view of an electromagnetic TGT calorimeter in a collider detector.

elements") of limited size (typically $60 \times 40 \times 1.6\, cm^3$) are the basic building blocks of the calorimeter. When assembled to form a calorimeter, they do not necessarily need to be parallel, thus yielding e.g. the structure of Fig. 2 Each absorber element is an independent mechanical and electrical entity. It consists of a few (e.g. four) absorber plates. It can be tested independently prior to installation and can be replaced during the whole construction phase without dismounting the calorimeter. Given the rather large size and the high degree of complexity of calorimeters at future colliders, this aspect is of utmost importance. In addition, the simple mechanical structure eases design and construction.

The planar structure of the individual absorber elements and their limited size allows to use standard copper coated readout boards with no limitation concerning the pad structure. Combined with the independence of the absorber elements, this offers a large flexibility of the pad segmentation (both along the shower axis and transverse to it). In particular, special fine segmentation can be incorporated at any given depth along the shower axis. It allows for optimization of the calorimeter performance for electron identification, for angular measurement of photons, for resolution of two photons (i.e. for the tagging of π^0), and for resolution of the overlap of photons with charged pions. An extension of the readout board beyond the front of the absorber plate gives the possibility to measure the energy of a particle which started showering in material in front of the calorimeter ("presampler" of Fig. 1), thus offering a way to integrate a preshower detector for energy correction.

The charge collection time at future collider experiments is a critical issue. Therefore the requirements on the charge transfer from the electrodes to the preamplifier are rather strict. In the TGT concept, the preamplifiers are integrated as VLSI chips in the absorber elements close to the signal source. Modules of summing amplifiers and signal shaping, which form the readout channels and trigger towers, are placed on the outside of the calorimeters, but still in the LAr. This offers once more a high degree of flexibility for combining individual pad structures to readout channels.

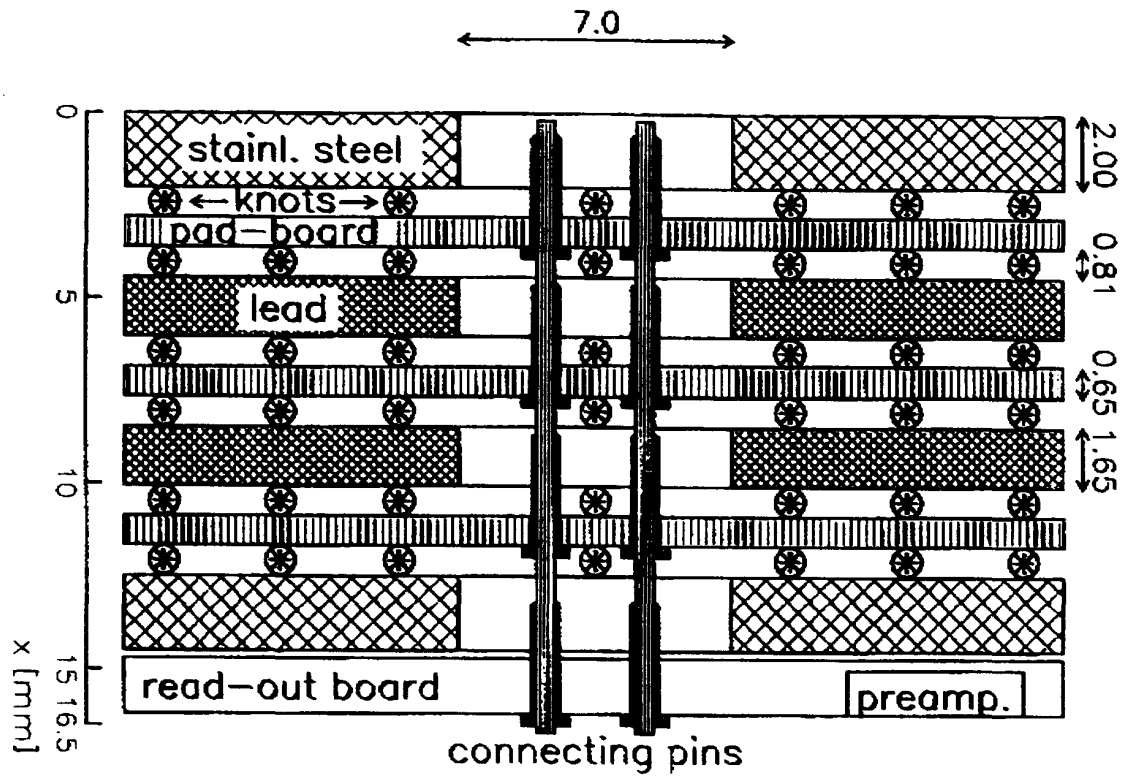

Figure 3: Cross-section of one absorber element showing how the contacts between all padboards and the electronics multilayer board are made.

2.2 The Calorimeter Structure

As pointed out, a TGT calorimeter is assembled out of a series of identical absorber elements, an example of which is given in Fig. 2. In Fig. 3 a detail of the cross-section for a single absorber element in the vicinity of the electrical connection is shown. It consists of four absorber plates, three double gaps of 2×0.8 mm LAr with readout electrodes ("padboards") in the centre, and at the end a multilayer electronics board (~ 1.2 mm thickness) which carries preamplifier and calibration chips. The two outer absorber plates consist of 2.0 mm stainless steel and the two inner plates are made of 1.65 mm lead. The stainless steel plates provide the mechanical stability and their thickness has been chosen to maintain a constant sampling fraction. The whole absorber element is held together by bolts with threads and with screws. The bolts are located at the center and around the circumference of the plates and boards at typical distances of 15 cm from each other. As shown in Fig. 3, the pads of three consecutive double gaps are electrically connected in parallel to each other and to the multilayer board on which the corresponding preamplifier channel is mounted; they constitute the basic "readout cell".

The LAr gap width is maintained by spacers and a mesh covering the active area. The mesh is made of polycarbonate and has knots arranged in squares of $20 \times 20\,\mathrm{mm}^2$. These knots are precisely rolled to a thickness of 0.8 mm. The filaments connecting the knots have a diameter of 0.2 mm.

A cross section of the readout electrode is shown in Fig. 4. The boards consist of a 0.45 mm G10 plate clad on both sides with copper pads (Cu thickness $35\,\mu m$), an insulating kapton layer (thickness $50\,\mu m$) and a coating ($\sim 20\,\mu m$) of high electrical resistivity to be put at high voltage (typically 800 V).

Table 1 summarizes various parameters for one readout cell.

Table 1: Parameters for one readout cell.

Argon gap width	$6 \times 0.8\,\mathrm{mm}$
Pad	$42.5 \times 30\,\mathrm{mm}^2$
Spacing between pads	$0.3\,\mathrm{mm}$
Detector capacity	120 pF / 3 double gaps
HV decoupling capacity	4800 pF / 3 double gaps
Dead area	$\leq 1\,\%$
Thickness	$0.89\ X_0$
Geometrical Thickness	$16\,\mathrm{mm}$

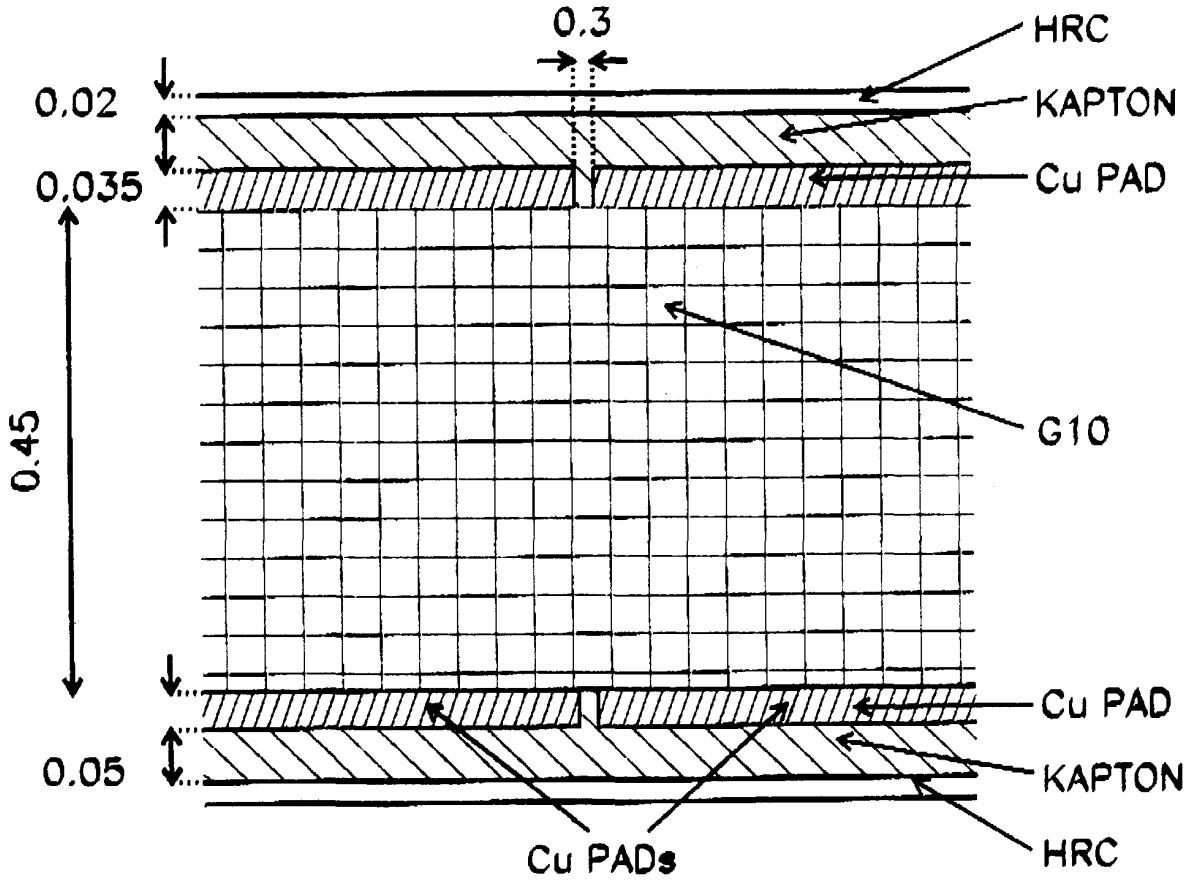

Figure 4: Cross-section of the padboard.

The segmentation of the calorimeter along the shower axis is obtained by electronically summing consecutive readout cells on different absorber elements.

In order to reconstruct isolated single photons with high precision, both a good angular resolution and a good rejection against high energy π^0's ($\sim$100 GeV) are required. Therefore some readout pads are divided into strips typically located after $\sim 2.5-5\ X_0$, as is also indicated in Fig. 1.

3 The Test Set-up

3.1 The TGT Test Module

A calorimeter test module of transverse dimensions $42.5 \times 36\,\mathrm{cm}^2$ and of 25 radiation lengths (X_0) depth has been built, leading to nearly complete shower containment at SPS energies and allowing for studies of uniformity, linearity and resolution.

The calorimeter consists of 36 identical absorber elements with a thickness of 0.89 X_0 each, mounted on a mechanical structure which was inserted as a whole into a cryostat. Fig. 5 shows a schematic view of this assembly. The orientation of the absorber elements changes continuously, reflecting the concept of constant impact angle of 45° when mounted in a collider detector. The details of the proposed set-up were fixed according to a detector configuration in a barrel calorimeter of a collider experiment and with a view to the neccessary performance of such a calorimeter [6].

The absorber elements were constructed as described above. Originally it was planned to clad the lead plates with 0.1 mm stainless steel foils. However, it turned out that the extensive machining of the clad plates resulted occasionally in unacceptable surface distortions. Therefore we decided to use for the first phase measurements bare lead plates, which caused sometimes severe high voltage problems: Six of the 108 double gaps drew such high current at the operational voltage of 800 V that they had to be disconnected.

The layout of the pads on the padboard is schematically presented in Fig. 6. The 120 pads have an identical size of $42.5 \times 30\,\mathrm{mm}^2$, separated by 0.3 mm. Viewed under an incident angle of 45°, their shape appears quadratic ($30 \times 30\,\mathrm{mm}^2$). This size would correspond to a minimal angular granularity in pseudorapidity and azimuth of $\Delta\eta \times \Delta\varphi = 0.02 \times 0.02$, calculated for a barrel calorimeter of a collider detector at a radial distance of 1.5 m from the interaction point. The interconnected pads of the three double gaps inside an absorber element form the basic readout cells. The connections are always done at the center of four cells in order to minimize the inactive area. They are shown in Fig. 6 together with the positions of the bolts and screws which hold the structure together. The inactive area is $\leq$ 1 % dominated by the high voltage guard zones around the pad interconnections. Their size is also indicated in Fig. 6.

Table 2: Results from measurements of various parameters of plates and boards.

Thickness of steel plates	2.000 ± 0.015 mm
Thickness of lead plates	1.647 ± 0.036 mm
Thickness of padboards	0.645 ± 0.009 mm
Gap width = diameter of mesh-knots	0.811 ± 0.022 mm
Pad capacity of double gap (air)	28.5 ± 1.2 pF
Surface resistivity	$\sigma = 2 - 20 M\Omega/\Box$

In the test module, two different modes of readout are used: In one part of the test module each readout cell is treated individually. In the other part a longitudinal segmentation of the calorimeter

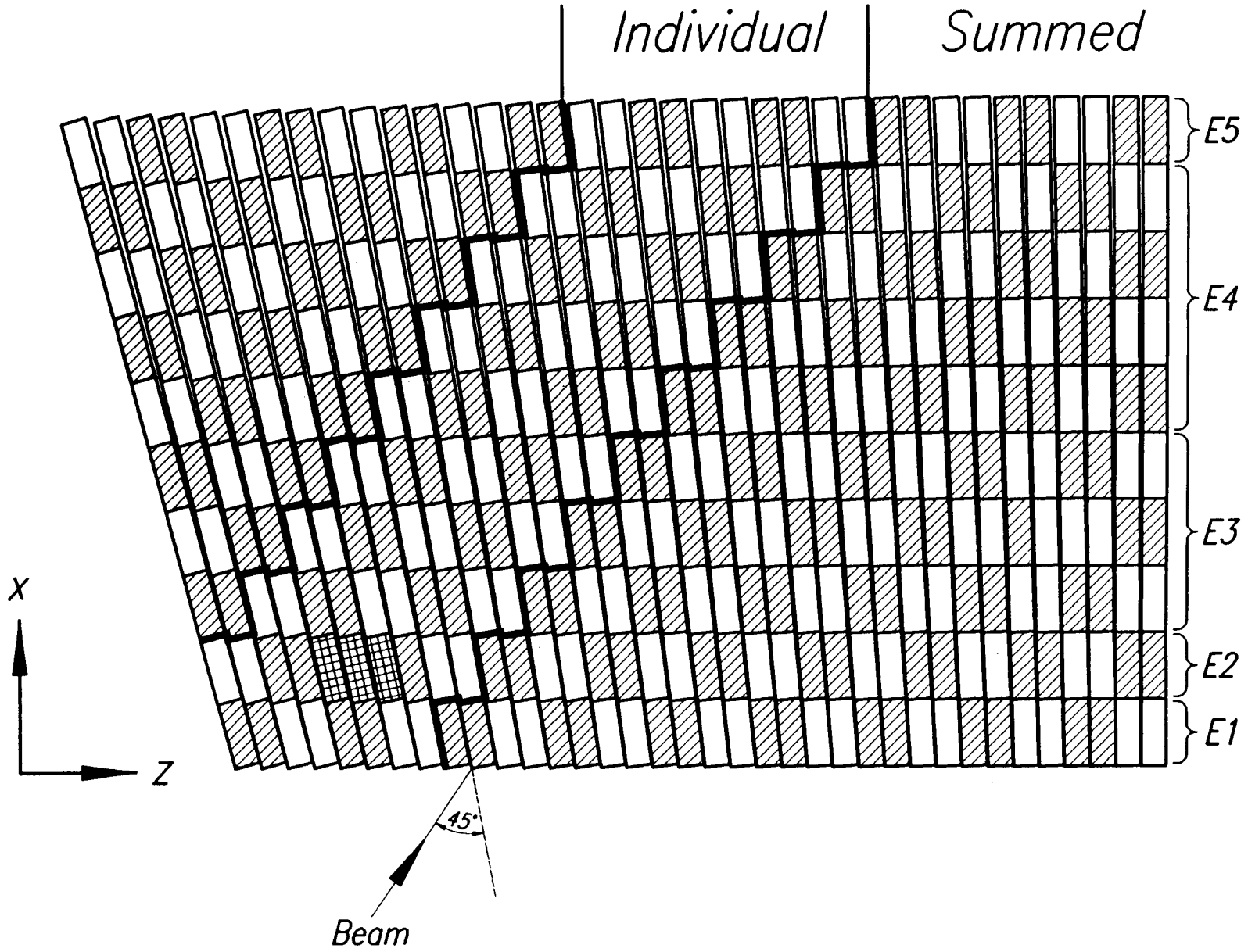

Figure 5: Schematic view of the test module. The cross-hatched pad-groups are equipped with strips. The areas of individual and summed readout are marked. E1 – E5 indicate the longitudinal segmentation.

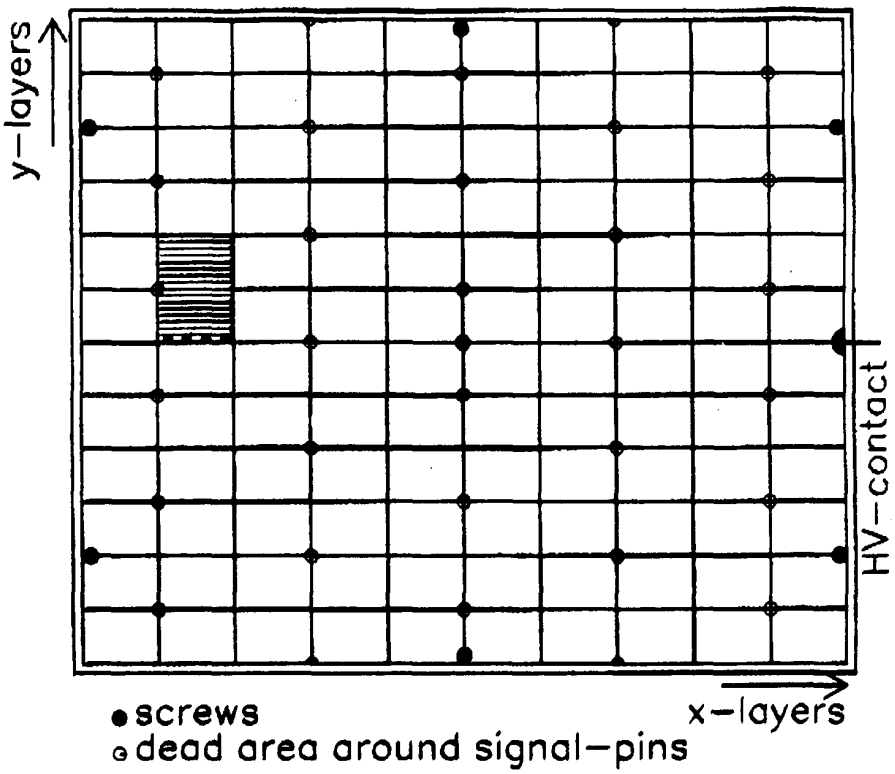

Figure 6: Segmentation of the padboard. The holes for the bolts with screws are marked A, B, and C, respectively, X denotes the location of the electrical connections.

is formed. Here the basic building block is the sum of two readout cells in the equivalent position in two adjacent absorber elements. Appropriate pairs of readout cells are electronically summed to point along the shower axis. Hence, the sum consists of one pair, three or four pairs of readout cells, forming readout channels E1 – E5 of Fig. 5 . which have different length along the shower axis. The segmentation and the two separate parts of the test module are indicated in Fig. 5.

The test module contains three absorber elements, where an area corresponding to two pads is divided into strips. For each of the three absorber elements, the strips run horizontally on the first padboard and vertically on the second, while the third one contains the usual pad. The vertical (horizontal) strips are 59.7 (42.2) mm long, 5.0 (3.45) mm wide and have a spacing of 0.3 mm. This finer grain subdivision is situated in the test module at a depth along the shower axis of $2.5-5\ X_o$.

The mechanical tolerances for the elements of the test module can be seen in Table 2 where the thickness measurements of the lead plates, the padboards (including copper, insulating foil and resistive coating) and the gap width together with some other relevant parameters are summarized. Especially from the variation of the gap width (r.m.s. $= 20\,\mu m$) the variation of the charge deposit can be estimated to be negligible (e.g. for a 40 GeV electron-initiated shower σ_Q/Q amounts to ~ 0.2 %).

In summary, it has been demonstrated that a calorimeter can be built with the TGT technology. All dimensions and tolerances of the thin gap configuration have been realized for the large number of absorber elements of this test. The only remaining problem were whiskers on the lead surface leading to HV problems in isolated areas.

3.2 The Electronic System

Figure 7 shows the layout of the electronic chain as used during the testbeam measurements. It consists of preamplifiers connected to the individual readout cells, summing amplifiers (where the

readout channels are formed), shaping amplifiers, a multiplexed readout system, and a calibration system. The design of this electronics is based partly on commercially available elements and partly on designs by the H 1 collaboration, with the exception of the summing and merging electronics.

The signals collected from the LAr cells are fed into charge-sensitive preamplifiers [7] which are located within the cryostat inside of an isolating box in the cold argon gas at a distance of $\sim 1\,\mathrm{m}$ from the pad. The temperature inside the box is continuously measured at 9 locations and is regulated to stay constant within 10 degrees.

The signals are transmitted via 8 m long flat cables of $50\,\Omega$ impedance to the outside of the cryostat where they are fed into summing amplifiers placed on summing and merging boards located on the top of a platform close to the cryostat. The role of these boards is to add the signals from single preamplifiers to form readout segments which point along the shower axis. Up to eight readout cells are summed together longitudinally to form a readout channel. For this purpose, signals from respective readout cells are merged at the input of a summing amplifier. The signals from 16 summing amplifiers each are sent to a signal processing module which is located close to the cryostat as well. Here the signals are shaped (peaking time $t_p = 500ns$), sampled and, after multiplexing, sent further to ADCs with 12 (14) bit resolution for large (small) signals, respectively. The receiving part of the multiplexed readout and the ADC system are located at a distance of 60 m in the experimental control room. The description of the readout part of the electronics using the multiplexed H 1 readout system may be found in [8].

In the same signal processing module, additional amplifiers form the trigger segment which consists of four readout channels summed in the plane transverse to the shower axis. On every module there are four summing amplifiers with four inputs each. Therefore four trigger segments are available at the output of each group of 16 readout channels. These signals are then sent to a summing stage where trigger towers are formed, each consisting of the sum of five trigger segments. The trigger tower signals are digitized in a fast (25 ns) FADC system to provide input for a special calorimeter trigger [9].

We have employed the calibration system as set-up by H 1 [10]. All preamplifiers are pulsed at the same time by injecting voltage pulses of appropriate shape into capacitors which are mounted on the multilayer board on the backside of the absorber elements. These capacitors were selected to a precision of $\pm 0.5\,\%$ corresponding to the required precision of the calibration system. For each readout channel the pulse level is varied such that the full dynamic range of the ADC is exploited avoiding saturation effects in the summed readout channels. In order to obtain cross-talk corrections, each preamplifier is also pulsed individually.

A fitting procedure with four parameters is used to compute the charge Q from the ADC counts x:

$$Q = P_0 + P_1 x + P_2(P_0 + P_1 x)^2 + P_3(P_0 + P_1 x)^3.$$

Most important is the linear term P_1 which is usually referred to as 'gain' parameter. Three groups of channels with different gain parameters are distinguished: The readout cells, the strip channels, and the summed channels. Within each group the gains are reasonably uniform, except for the single pad channels where two groups with slightly different gains were found which is attributed to different lots of electronic components. Within each group the gains show a spread of $\sim \pm 2\,\%$, which leads to an r.m.s. of the total distribution of $\pm 4.5\,\%$.

As is specific to the TGT amplifier scheme, the outputs of several preamplifiers are fed into the same shaping amplifier and readout channel. For the successful application of this scheme it is preferable to have only small gain variations between the individual inputs. Calibration data obtained with individual pulsing have been used to measure the uniformity of the preamplifiers within the same readout channel. For each channel the average preamplifier gain (μ) as well as the r.m.s. (σ) spread around this mean value have been determined. The ratios σ/μ are formed separately for the four groups of summed channels, corresponding to two, six and eigth inputs. Only in the case of a large number

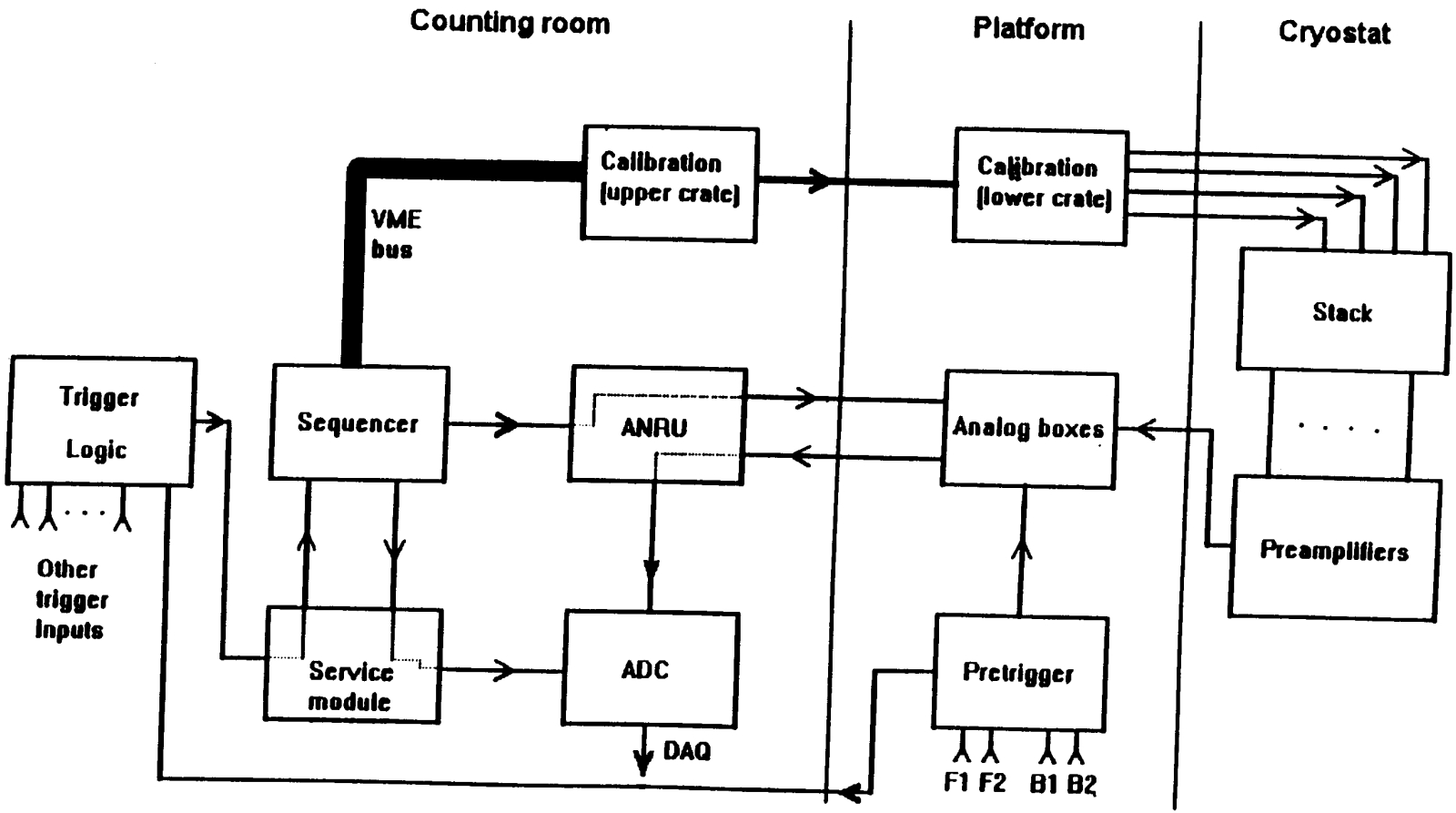

Figure 7: Layout of the electronic chain.

of inputs the mean value is a realistic measure of the true gain variation. From the distribution of the six and eight input channels one can deduce that in a realistic experimental application the individual gains vary at the level of $\pm 1.2\,\%$. From Monte Carlo studies it is known, that this corresponds to a contribution to the constant term of the energy resolution of well below 0.4 %.

4 Testbeam Results

The TGT module has been exposed to electrons, pions and muons in the energy range 20 - 200 GeV. These tests with beam offer the opportunity to study the homogeneity of the calorimeter response. Substructures even at the level below 1 cm can be investigated with muons. Electrons offer the opportunity to uncover variations in the response with very high precision, but on a larger scale in space, typically one Molière radius (2.2 cm). The comparison with Monte Carlo (MC) studies can finally help to disentangle mechanical effects from electronic performance ones.

Test data have been obtained in two run periods, the first one giving priority to scans using muons, the second one to scans using electrons. The momentum resolution of the electron beam is typically 0.5 %.

4.1 The Testbeam Set-up at CERN

Beam tests were performed with a separated beam (H6) of the CERN SPS. A large part of the equipment used was originally installed by the H 1 collaboration. The testbeam set-up is schematically shown in Fig. 8. The test module is located in a cryostat with an inner diameter of 2.50 m and a usable height of 2.00 m. The cryostat can be moved horizontally by ± 30 cm. A magnet allows to deflect the beam vertically by ± 25 cm at the entrance of the cryostat. As a result, a large area of impact positions of typically $60 \times 60\ cm^2$ can be scanned. The beam trigger set-up consists of three scintillator walls, of a differential Cerenkov counter for particle identification, and of two scintillation counters for fast timing (resolution $\sigma = 70$psec) [11]. Six multi wire proportional chamber (MWPC) planes with 1 mm wire spacing allow a precise measurement of impact position and angle.

4.2 Studies with muons

Data from extensive scans with muons along horizontal and vertical lines in the calorimeter have been taken to study the response to minimum ionizing particles. The muon signal is expected to be constant and thus provides a powerful tool to study the homogeneity of the calorimeter response. In addition, the inter-channel calibration in the range of low signals can be checked very effectively.

As mentioned above, in this test some high voltage problems had to be corrected prior to any analysis. A detailed muon analysis can yield correction factors for individual absorber elements or even for individual readout cells of a given absorber element. Comparing the muon and electron data of the first run period only, it turns out that the correction factors obtained from the muon data are compatible with those obtained from the electron data using the multi-parameter fit method as described in the following.

The expected muon signal in a given readout cell can be calculated, using the information from the MWPCs and the position of the readout cells. Only those muon signals were kept where the muon traversed the full absorber element within one readout cell. The mean value of this signal is expected to stay constant with time. In order to determine the muon signals, the pedestals have to be subtracted. As for the analyses discussed below, this subtraction has been done using random triggers taken in parallel with the data during each run. In order to be less sensitive to fluctuations in the Landau tail of the muon signal, a cut rejecting this tail has been applied. More details may be found in [12, 13].

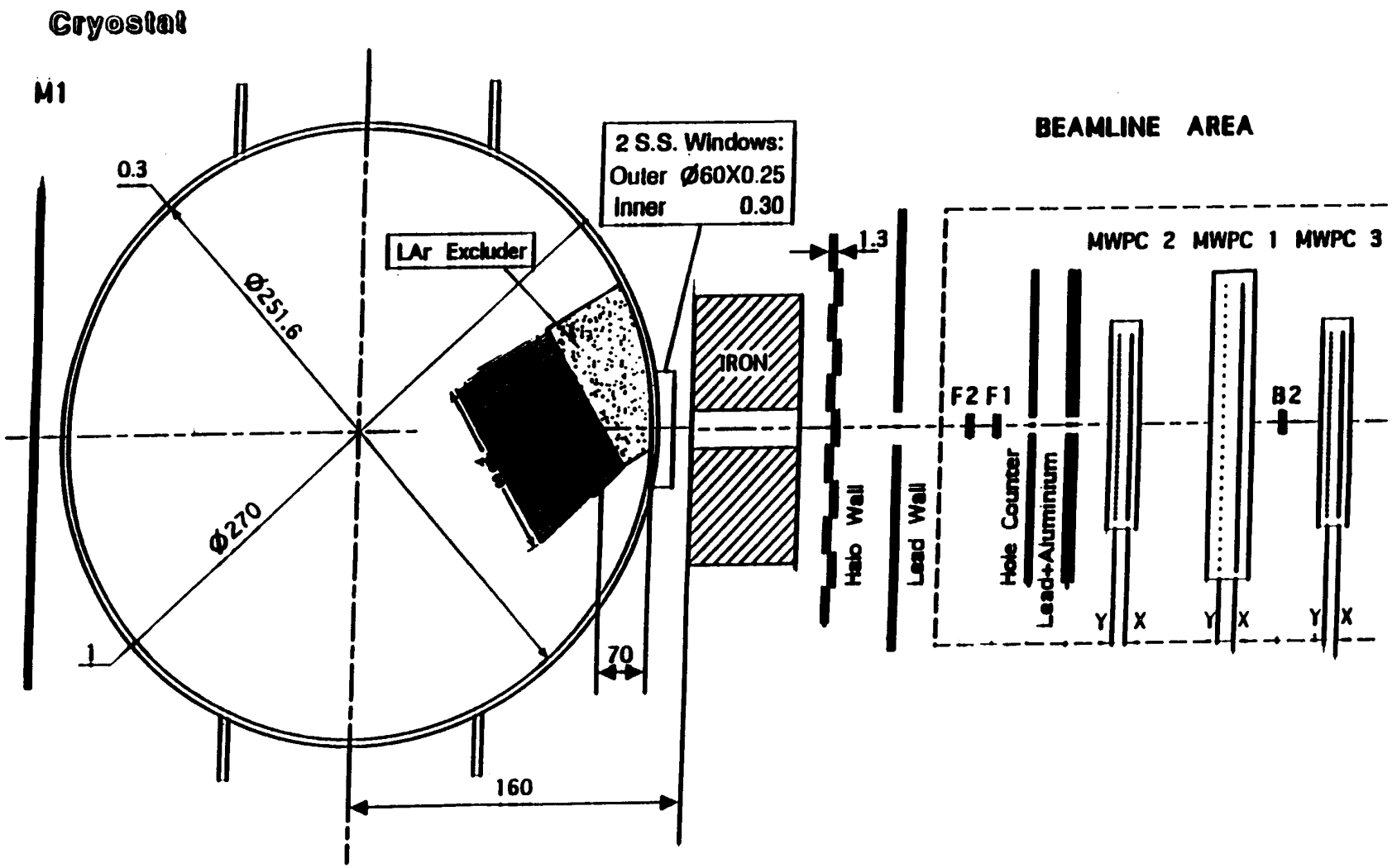

Figure 8: Set-up in the H6 beam line.

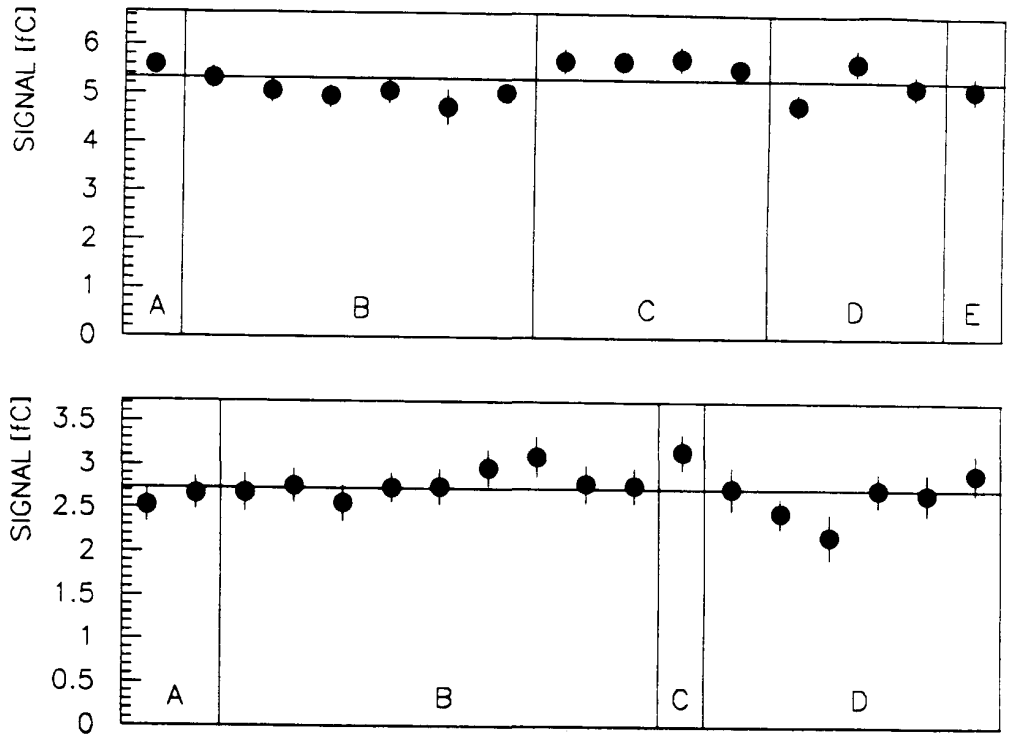

Figure 9: Top: Mean muon signal for five readout cells (A – E) of a standard absorber element. Bottom: Mean muon signal for four readout cells (A – D) of an absorber element which is affected by high voltage problems. Multiple entries refer to different data–taking runs. Shown are the statistical errors only.

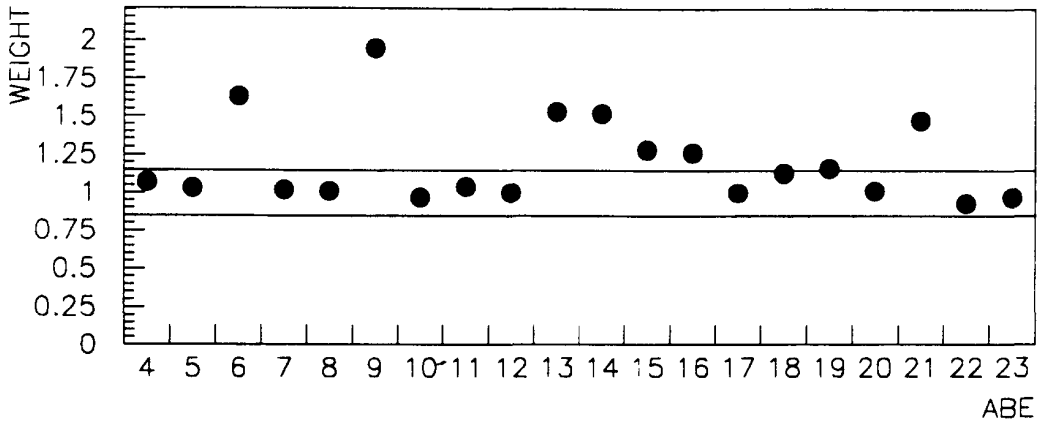

Figure 10: Mean weight for individual absorber elements as given by the average muon response with absorber element 12 as reference.

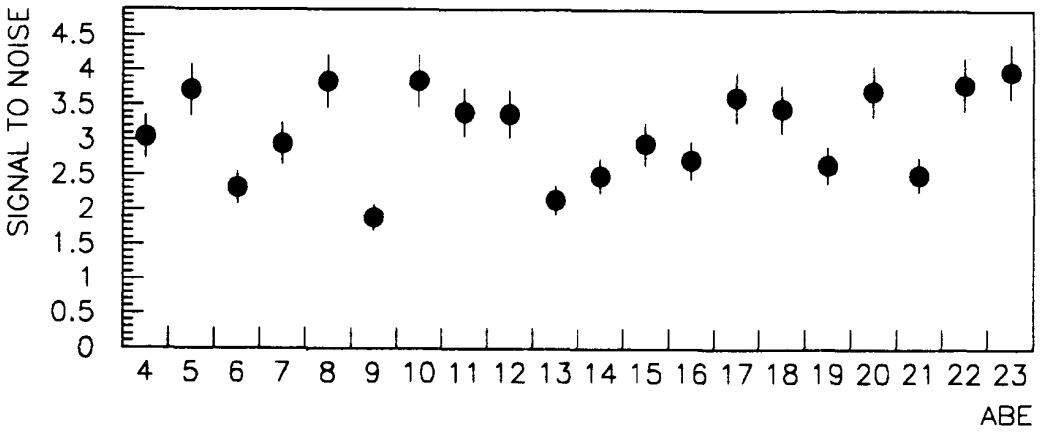

Figure 11: Average ratio of the muon signal and the electronic noise for different absorber elements. The errors shown are the statistical errors only.

As an example, Fig. 9 shows the mean value of the muon signal for five readout cells (labeled A – E) of a standard absorber element. The variation of the data referring to the same readout cell gives an indication of the systematic error due to the method used: It is typically of the order of 10 %.

In contrast, the absorber element shown at the bottom is affected by high voltage problems. The signal is reduced by typically a factor of two. Within the systematic error quoted this reduction is constant for all readout cells of this absorber element. This observation holds for all absorber elements affected by high voltage problems. The variation of the data for different readout cells in the same absorber element are always small compared to the difference between the mean signal from a good and a bad absorber element.

In order to correct for the high voltage problems, an average weight factor for each absorber element affected by these problems can be extracted from the data. Figure 10 shows the resulting weights of all absorber elements with absorber element 12, which has no high voltage problems, as reference. The statistical errors from the mean value of one absorber element are smaller than the points shown in Fig. 10. The data outside the 10 % systematic error band are from those absorber elements which are affected by high voltage problems.

For the muon response the signal to noise ratio is an important quantity. The average value of this ratio for the individual absorber elements is shown in Fig. 11. Here the signal has been divided by the r.m.s. of the noise distribution as obtained from random trigger signals. This ratio is typically bigger than 3 for the absorber elements not affected by high voltage problems.

In order to reconstruct the trajectories of muons, a special algorithm was developed where only information from the calorimeter was used. Cluster centers of charge deposit were formed seperately for every slice in x yielding up to 10 coordinate points. Cuts were applied in order to minimize the effects of noise on the resolution. An efficiency of 82 % was achieved with only 1.7 % of the random trigger events wrongly reconstructed as muons. The spatial resolution was determined by subjecting the points to a linefit, calculating the intersection with the front face of the calorimeter and projecting the resulting coordinate onto the MWPC plane. On average a spatial resolution of $\sigma_z = 0.53$ cm and an angular resolution of $\sigma_\vartheta = 1.0^0$ were obtained.

4.3 Studies with electrons

Electron data have been taken at 20, 40 and 80 GeV at various horizontal and vertical positions. In vertical direction the individually instrumented region is not big enough to perform a meaningful scan of the calorimeter without being affected by lateral leakage. Therefore we focus in this analysis on the data taken at a fixed vertical (y) position while varying the z position of the impact point and the energy of the electron beam. In order to reconstruct the electron energy, the calorimeter signals of 3 × 8 readout cells were added corresponding to an area of 9 × 12 cm.

The calibration constants which convert the deposited charge to the energy of the incident particle can be obtained by properly normalizing the electron data taken at various impact positions and energies, or, equivalently, by minimizing the energy resolution for all data runs simultaneonsly. The data analyzed here were affected by high voltage problems in six absorber elements. The corresponding correction factors have been determined from a global seven parameter fit, minimizing simultaneously the energy resolution for all runs taken. One parameter reflects the overall normalization and six parameters correspond to the correction factors for the absorber elements affected by the high voltage problems. This correction method has been tested with simulted data: The signal in the relevant absorber elements has been reduced by the corresponding factor. The energy resolution for the simulated data (at different energies) has again been optimized from a fit using calibration parameters for individual absorber elements. From fits varying the overall number of affected absorber elements and the absorber element position, exactly those absorber elements with the reduced signal could be localized. The related correction factors have on average been reproduced within 4 %. This demonstrates that, even though there is a strong correlation between neighbouring absorber elements due to the shower shape evolution, this method yields a unique set of correction factors with the required precision.

4.3.1 Energy resolution and uniformity of response

Figure 12 shows the measured energy distribution for electrons of 20, 40 and 80 GeV, for a fixed z position. A Gaussian fit (solid line) used to extract the energy resolution σ is shown as well.

Using random trigger events, an average electronic noise of 282 MeV in the 3 × 8 readout cell region has been measured. Thus the energy (E in GeV) resolution can be parameterized by:

$$\frac{\sigma(E)}{E} = \sqrt{p_1^2/E + p_2^2 + (0.282/E)^2}$$

The two parameters, the sampling term p_1 and the constant term p_2, can be obtained from a fit to the energy dependence of the energy resolution. As an example, Fig. 13 shows the energy resolution $\sigma/\sqrt{E}$ for four runs taken at a fixed z position yielding $p_1 = 11.5 \pm 0.3\,\%$ and $p_2 = 0.6 \pm 0.1\,\%$. The corresponding result from a fit to all data at various z positions and energies yields $p_1 = 11.0 \pm 0.3\,\%$ and $p_2 = 0.7 \pm 0.1\,\%$. An identical analysis has been carried out for a set of simulated data where all details of the present set-up have been taken into account, except for the material in front of the calorimeter. The corresponding result fitting the energy resolution yields $p_1 = 9.2 \pm 0.3\,\%$ and $p_2 = 0.5 \pm 0.1\,\%$. We attribute the difference of 2 % in the sampling term to the additional material in front of the calorimeter.

The linearity of the response for the four runs mentioned above is shown in Fig. 14. Without any further correction for dead material in front of the calorimeter (in total $0.67X_0$) the response is constant within 1 %.

The dependence of the energy resolution $\sigma/\sqrt{E}$ and the response on the horizontal impact position is shown in Figures 15 and 16 respectively for the electron data at 40 GeV. In the range covered,

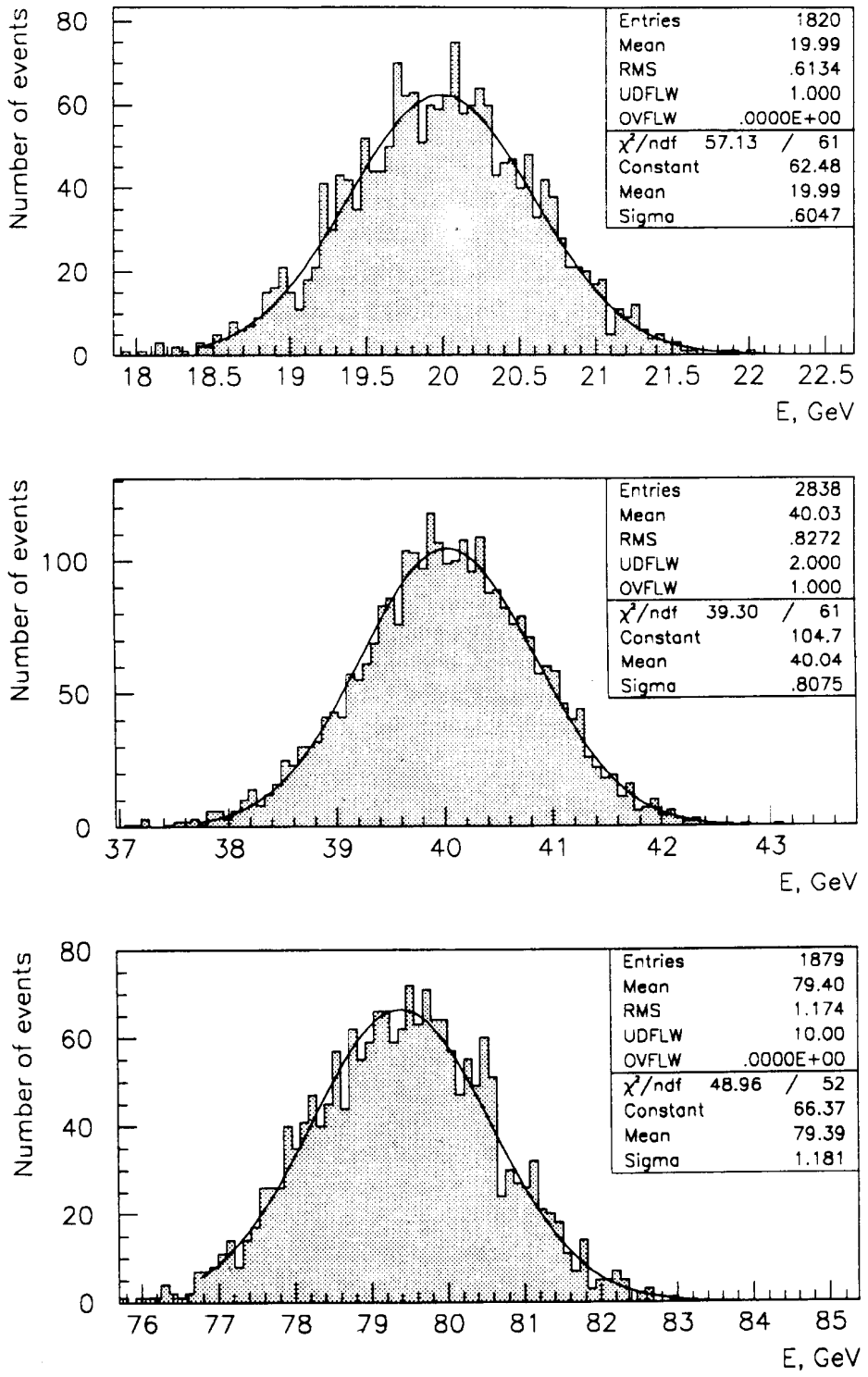

Figure 12: Energy deposition for electrons at a given horizontal impact point for three runs at energies of 20, 40 and 80 GeV.

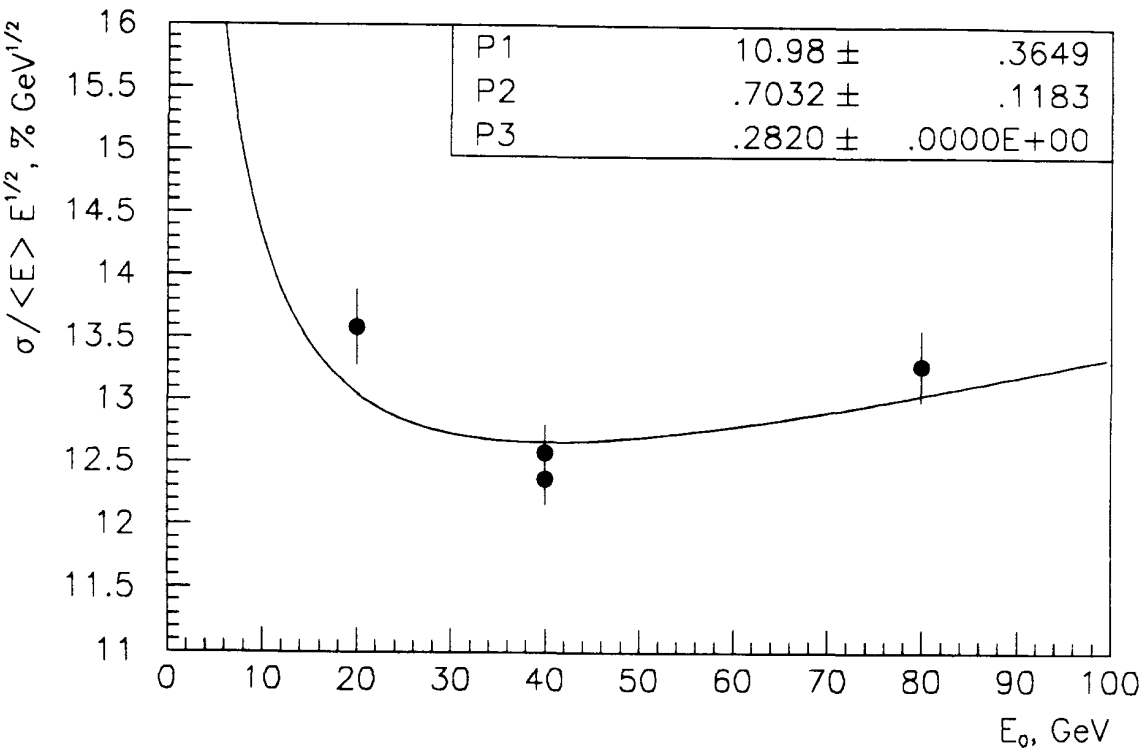

Figure 13: Energy resolution $[\sigma/ < E >] \cdot E^{1/2}$ for electrons of 20, 40 and and 80 GeV at a fixed impact position. The full line represents a fit to the data points with $\sigma/ < E >= [p_1^2/E_0 + p_2^2 + (0.282/E_0)^2]^{1/2}$ where E_0 is the beam energy.

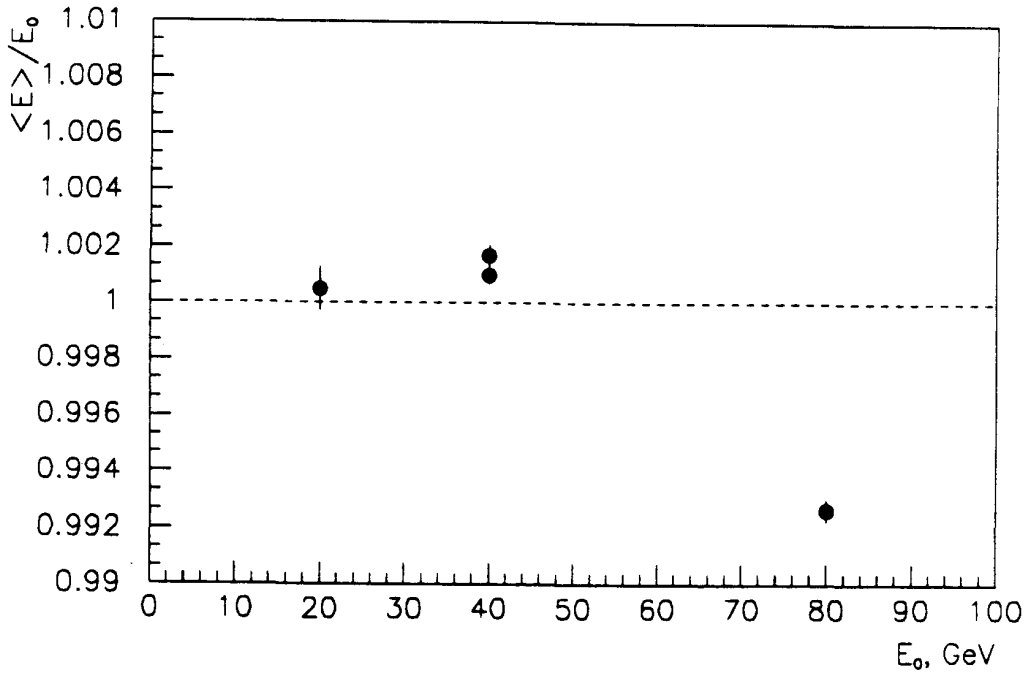

Figure 14: Linearity of the energy response for electrons of 20, 40 and and 80 GeV at a fixed impact position. Shown is the ratio relative to the average response.

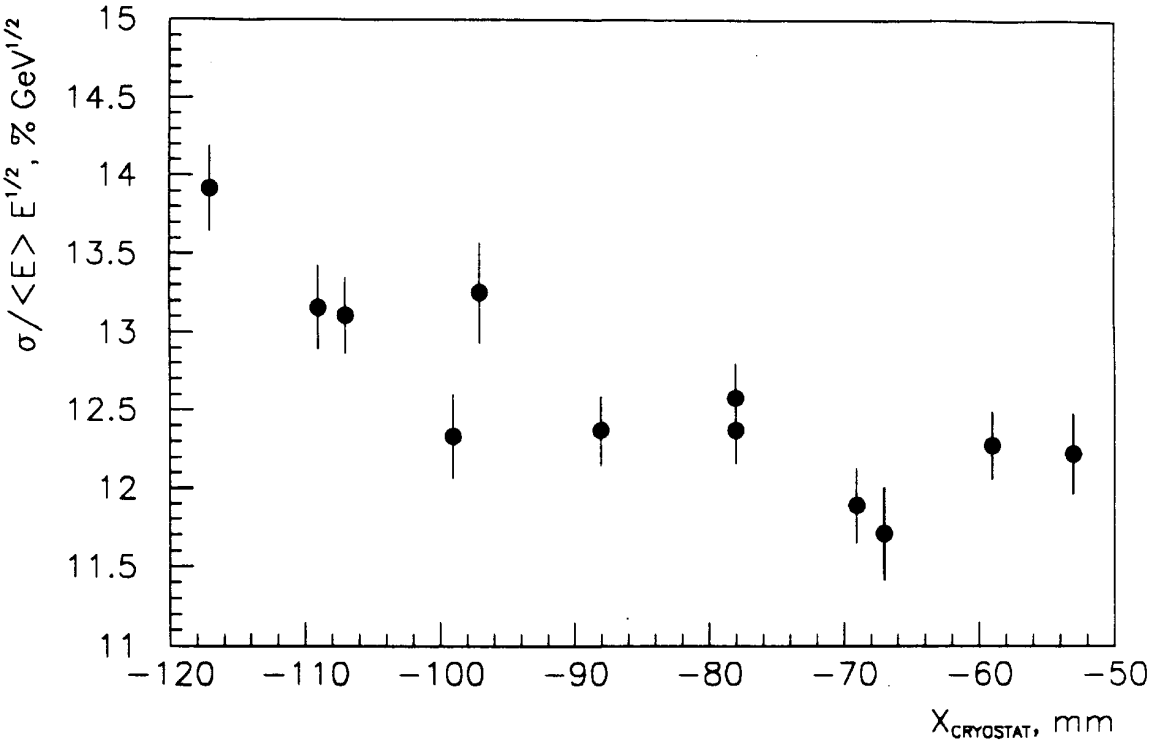

Figure 15: Dependence of the energy resolution $[\sigma/ < E >] \cdot E^{1/2}$ on the horizontal impact position z for electrons of 40 GeV.

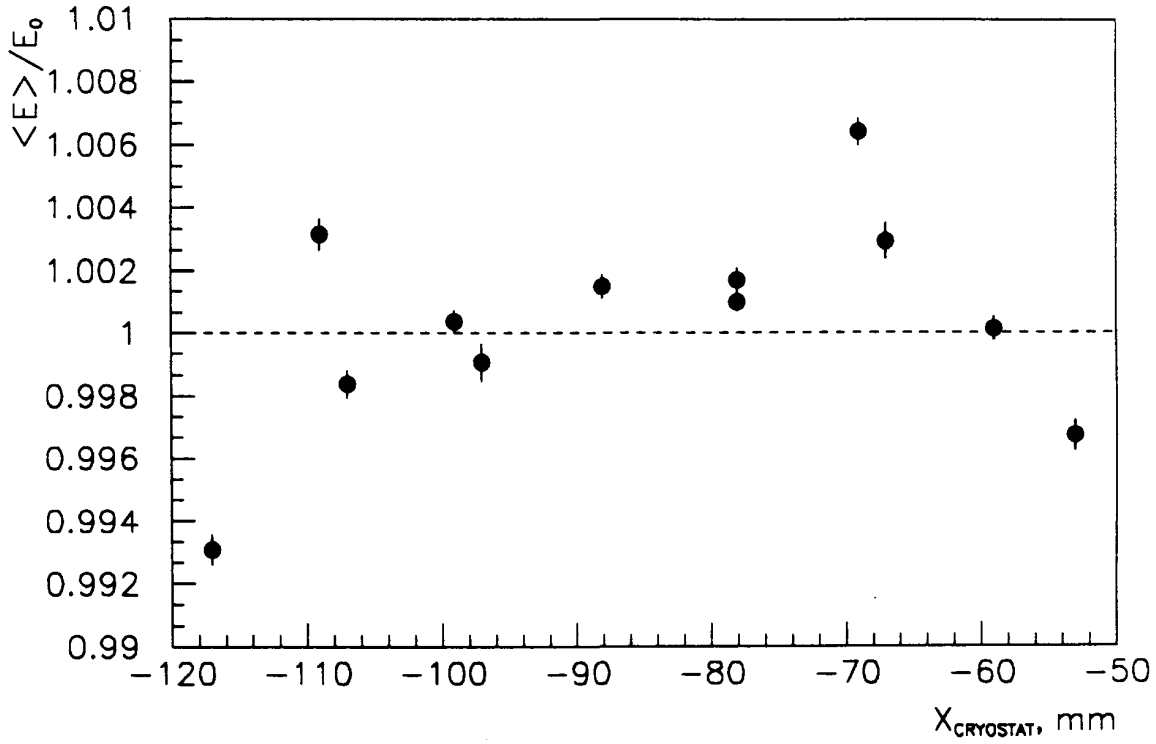

Figure 16: Dependence of the energy response on the horizontal impact position z for electrons of 40 GeV. Shown is the ratio relative to the average response.

the response stays within $\pm 0.7\,\%$. The data point at $z = -117$ mm seems to be affected by lateral leakage. An indication for some leakage at this point might also be seen in the energy resolution, which is somewhat worse at this point. For the other data points the energy resolution does not show any strong variation within the error.

4.3.2 Angular resolution

The electron shower axis has been determined from a straight line fit to individual cluster centres. The clusters have been formed separately for slices in x and y, and for individual absorber elements. In addition, the strip information from the x and y orientation may be combined to a cluster as well. In order to obtain the cluster centre, the energy weighted centre from the related readout cells has been calculated. The granularity due to the pad structure leads to a systematic deviation of the reconstructed cluster centre from the nominal value as function of the cluster centre position. These fits have been done for all cluster types used in the reconstruction. The shower axis has been reconstructed from a straight line fit to these corrected cluster centres, using the cluster energy as weighting factor. The precision σ of the reconstructed cluster centre from a given layer has been used as an additional weight in the fit procedure. The x and y coordinates from the strip information have been obtained from a Gauss fit to the corresponding distribution of the data.

Up to 10 layers are available for the fit given the rather fine longitudinal segmentation (not yet including the strip information). For the straight line fit, clusters based on the longitudinal structure as well as such based on the individual absorber element structure have been used simultaneously, neglecting any correlation between these two sets. The systematic effects, as resulting from e.g. the high voltage correction factors, are thus averaged to some extent.

Neglecting the strip information, we obtain for the angular resolution of the shower axis $\sigma_\theta = 7.5$ (6.4, 4.8) mrad for electrons of 20 (40, 80) GeV energy respectively. This yields an angular resolution of $\sigma_\theta = 39.0/\sqrt{E}$ mrad (E in GeV) in the energy range considered. The corresponding result from simulation is $\sigma_\theta = 45.4/\sqrt{E}$ mrad (E in GeV). Adding the strip information improves the angular resolution typically by $\sim 10\,\%$.

In the final set-up a maximum of five longitudinal layers will be available. In order to predict the performance for this set-up, the readout cell information is regrouped to the appropriate structure. We obtain $\sigma_\theta = 39.0/\sqrt{E}$ mrad (E in GeV) without using the strip information. Again an improvement by $\sim 10\,\%$ is achieved when the strip information is added.

5 Conclusion

A novel concept for a LAr calorimeter for detectors at future high energy, high rate accelerators is described: the thin gap turbine (TGT) calorimeter. A detailed technical design of such a calorimeter has been made, as described here, and a test module has been constructed accordingly. Its basic idea – the modular construction of a collider detector from single, independent absorber elements – is verified in a test module of reasonable size. It is thus demonstrated that a complicated detector structure, e.g. with pointing geometry, can, in principle, be assembled in this way. The mechanical problems of such a concept, in particular the thin gap structure of constant width and of tight tolerances, could be solved in a satisfactory way for a large number of absorber elements. The small problem remaining, high voltage breakdowns in isolated plates, can be attributed to the fabrication of the lead sheets. Also the ultimate goal of the concept, the use of fast, monolithic GaAs electronics directly at the detector, could partially be tested in a successful way by placing the slower electronics of this test stage in the cold argon gas.

The results from an exposure to testbeams of muons, electrons and pions has yielded results in agreement with the expectations. In particular, the spatial uniformity of response, the energy resolution and the angular resolution agree well with the predictions from simulation.

References

[1] ATLAS Collaboration, Letter of intent for a General-Purpose pp Experiment at the Large Hadron Collider at CERN, CERN/LHCC/92-4 (1992).

[2] D0 Collaboration, M. Abolins et al., *Nucl.Instr.&Meth.* **A280** (1989), 36.

[3] H 1 Calorimeter Group, B. Andrieu et al., The H 1 Liquid Argon Calorimeter System, *Nucl.Instr.&Meth.* **A336** (1993), 460.

[4] RD3 Collaboration, B. Aubert et al., CERN/DRDC/90-31 (1990).

[5] RD33 Collaboration, C. Berger et al., Proposal CERN/DRDC/93-02 (1993).

[6] M. Aderholz et al., Expected Performance of the TGT Calorimeter, ATLAS Note CAL–NO–22 (1993).

[7] Deutsche Vitrohm GmbH, based on a design by MPI München.

[8] R. Bernier et al., LAL Orsay, H1 calorimeter electronics (between shaper and ADC), H 1 Note 07/92–237 (1992).

[9] RD 27 Collaboration, Proposal DRDC/P37 (1992).

[10] D. Breton et al., LAL Orsay, H1 calorimeter calibration electronics, H 1 Note 04/92–219 (1992).

[11] A. Dannenmann, Aufbau und Test von Szintillationszählern mit hoher Zeitauflösung, Staatsexamensarbeit Universität Heidelberg (1994).

[12] H. Frey, Untersuchungen zur Wechselwirkung von Elektronen und Hadronen in einem Flüssig-Argon-Kalorimeter für ein LHC-Experiment, Diplomarbeit Universität München (1994).

[13] D. Zerwas, Analyse der Myondaten des Thin Gap Turbinen Kalorimeters, Diplomarbeit Universität Heidelberg (1994).

[14] R. Brun et al., GEANT3, CERN Program Library Writeup W5013.

[15] H.U.Bengtsson and T. Sjostrand, PYTHIA, Comput. Phys. Comm. 46 (1987) 43.